01 Mar 2023

Particle Migration in Large Cross-Section Ceramic On-Demand Extrusion Components

Austin J. Martin

Wenbin Li

Jeremy Lee Watts
Missouri University of Science and Technology, jwatts@mst.edu

Gregory E. Hilmas
Missouri University of Science and Technology, ghilmas@mst.edu

et. al. For a complete list of authors, see https://scholarsmine.mst.edu/math_stat_facwork/1142

Recommended Citation

A. J. Martin et al., "Particle Migration in Large Cross-Section Ceramic On-Demand Extrusion Components," *Journal of the European Ceramic Society*, vol. 43, no. 3, pp. 1087 - 1097, Elsevier, Mar 2023.
The definitive version is available at https://doi.org/10.1016/j.jeurceramsoc.2022.10.059

Journal of the European Ceramic Society 43 (2023) 1087–1097

Contents lists available at ScienceDirect

Journal of the European Ceramic Society

journal homepage: www.elsevier.com/locate/jeurceramsoc

Particle migration in large cross-section ceramic on-demand extrusion components

Austin J. Martin [a,*], Wenbin Li [b], Jeremy Watts [a], Gregory E. Hilmas [a], Ming C. Leu [b], Tieshu Huang [c]

[a] Department of Materials Science and Engineering, Missouri University of Science and Technology, Rolla, MO, USA
[b] Department of Mechanical and Aerospace Engineering, Missouri University of Science and Technology, Rolla, MO, USA
[c] Kansas City National Security Campus, Honeywell Federal Manufacturing & Technologies, Kansas City, MO, USA

ARTICLE INFO

Keywords:
Additive manufacturing
Direct ink writing
Coffee-ring effect
Rheology
Printability

ABSTRACT

Ceramic On-Demand Extrusion (CODE) is a direct ink writing process which allows for the creation of near theoretically dense ceramic components with large cross-sections due to oil-assisted drying. Yttria-stabilized zirconia (YSZ) colloidal pastes (~$d_{50} \lesssim 1$ μm) were used in CODE to produce dense (multi-road infill and ≳ 98% relative density), large continuous volume (> 1 cm^3), and high fidelity (nozzle diameters ≲ 1 mm) structural ceramic components. However, many of these printed components underwent significant particle migration after forming. The reason for this particle migration defect was investigated using the coffee-ring effect for dilute solutions and rheological methods for dense suspensions. Modifications to the colloidal paste, such as changes in solids loading, pH, or surfactant concentration were explored as to their effectiveness to mitigate the defect. Ultimately, paste formulation and printing trade-offs are discussed with respect to the post-printing defect and as to general direct-write patterning.

1. Introduction

Additive manufacturing (AM) of ceramic components has gained increased interest because of the ability to form geometrically complex, 3D objects [1–6]. Spanning structures and small continuous volume (<1 cm^3), densely filled ceramic parts have been fabricated in the past [2], but limited research has been devoted to produce larger, densely-filled 3D components (≳ 1 cm^3) [7]. Producing defect-free ceramic components with continuous volumes >1 cm^3 tend to have uneconomically long post-processing steps (>1 week) such as drying or debinding[8]; the processing of objects >1 cm^3 also tend to be defect prone [9]. Numerous issues arise when attempting to print larger, dense cross-sections including cracking [10,11], particle or binder segregation [12–14] or migration [15,16], warping [17], and porosity [18–20]. The lower binder content (typically <10 vol%) used in most robocasting (RC) or direct-ink writing (DIW) processes allows for porosity-free debinding when compared to other ceramic AM processes such as stereolithography (SLA) or fused deposition of ceramics (FDC)[21]. Powder processing and pressing operations can result in high sintered densities (>99%), but for large cross-sections, stress gradients can become difficult to manage [22–24]. Wet processing methods typically involve lower pressure/density gradients than powder operations and offer greater microstructural controls [25–29]. Both SLA and FDC have post-processing limitations related to binder removal, similar to ceramic injection molding (CIM)[9], but these AM techniques have enabled customized, rapid manufacturing and higher fidelity objects than CIM (e.g., lattices)[30,31]. Ceramic binder jetting (BJ3DP) has produced larger volume parts (industrial build chambers ~700 cm^3 and greater; parts >1 cm^3), but typically has challenges reaching greater than 90% relative densities without infiltration, due to powder packing inefficiencies [32,33]. Although other ceramic additive manufacturing processes have created multi-material parts [34,35], DIW and related direct-write processes naturally allow for the integration of sub-structures [36], conformal printing [37,38], and graded material compositions [39–41]. Steps have been taken in past practices to avoid cracking and warping in robocasting by using an oil-bath and high humidity bulk drying [42], but to the authors' knowledge, particle migration was not experimentally observed for large continuous volume (>1 cm^3) 3D printed ceramic articles.

Ceramic On-Demand Extrusion (CODE) is a RC/DIW type process

* Corresponding author.
E-mail address: austin.martin@mst.edu (A.J. Martin).

https://doi.org/10.1016/j.jeurceramsoc.2022.10.059
Received 3 May 2022; Accepted 21 October 2022
Available online 28 October 2022

that utilizes colloidal pastes with a high ceramic volume fraction (typically $\varphi \geq 40\%$), an oil bath and controlled drying during deposition, followed by high humidity bulk drying to mitigate non-uniform drying [43–45]. However, particle migration was observed in 3D printed objects, especially in objects with large continuous volumes (>1 cm^3). Previously, a helical gear with a keyway was printed with a 3 mol% yttria-stabilized zirconia (3YSZ) paste using the CODE system (Fig. 1a) and sintered. The part was supposed to have the given cross-section presented in the computer aided design model shown in Fig. 1(b), but the part exhibited a tortuous hole (a defect) past the designed keyway (Fig. 1c). Similarly, for other parts printed with this paste, a visible hole was contained within the final part (Fig. 1d).

Lateral particle migration, as shown in Fig. 1, has notable, but less dramatic examples. The coffee-ring effect (CRE), termed by Deegan et al. [46], occurs due to the differential evaporation rate along a solution droplet containing insoluble particles. As the outer region of the droplet evaporates quicker due to differential curvature, a particle is pinned at the interface between the substrate, air, and solution. Capillary flow is induced as the remaining fluid from the inner regions of the droplet are wicked toward the outer regions of lower concentration (i.e., drier). Typically, the coffee-ring is a common detrimental deposit in printing technologies (esp. inkjet). Therefore, traditionally, the CRE has been studied in terms of developing methods to avoid it. However, applications have expanded toward utilizing the coffee-ring deposits for chemical diagnostics and material patterning [47].

This type of migration is not ideal when trying to precisely form dense, as-designed geometries. However, preventative quality controls have not been further explored for limiting particle migration during CODE processing. This research attempts to investigate the constraints on paste rheology and microstructural control for large cross-section CODE-printed parts. Therefore, the goals of this research were to understand how CODE contributes to particle migration; to investigate particle migration for these dense colloidal suspensions used in CODE by utilizing the dilute analogue – the CRE; to characterize the dense suspension behavior using rheology; to discuss suspension improvements to avoid particle migration; and finally, to discuss implications on paste formulation for dense, large cross-section, CODE-printed ceramic parts.

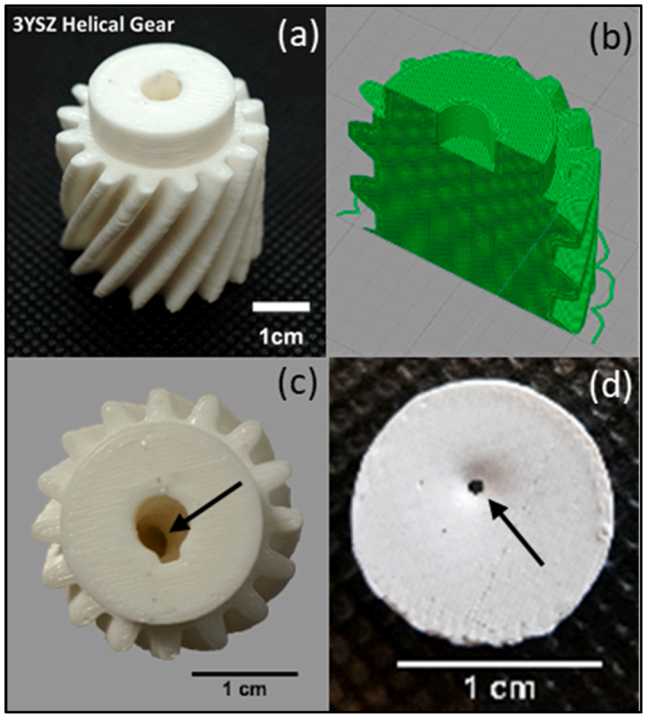

Fig. 1. (a) CODE printed and sintered 3YSZ helical gear, (b) CAD cross-section for the zirconia helical gear with a keyway, as designed, (c) Top view of the helical gear with an arrow pointing to the tortuous hole, (d) Another smaller, unsintered object with an arrow pointing to a small hole.

2. Experimental procedure

2.1. Coffee-ring experimentation

A seven by seven (7×7) matrix, consisting of 49 different solutions, was designed to assess the effect of pH and dispersant concentration on particle migration. First, seven 20 vol% zirconia suspensions were created using 3 mol% yttria-stabilized zirconia (3YSZ) (TZ-3Y-E, TOSOH USA, Inc., Grove City, OH, USA), deionized water (with one series utilizing distilled water as a control), and Dolapix CE 64 dispersant (65 wt% solution, Zschimmer & Schwarz Chemie GmbH, Lahnstein, Germany). The powder, water, and dispersant were ball milled using 3YSZ spherical (5.2 mm diameter) zirconia media in a high-density polyethylene (HDPE) bottle (125 mL, 5 cm diameter, Fisher Scientific, Hampton, NH, USA). In each of these suspensions, dispersant concentration was varied between 0 and 50 mg/g, corresponding to between 0 and 3.125 mg/m^2 for TZ-3Y-E (specific surface area of 16 ± 3 m^2/g, manufacture supplied). Each suspension was placed on a jar mill roller (U.S. Stoneware, East Palestine, OH, USA) at approximately 15 revolutions per minute for 24 h. A low number of revolutions per minute (<40) was chosen to allow the media to fall through the viscous paste and break agglomerates, not to drastically modify or reduce the particle size distribution.

Forty-nine (49) solutions were created by diluting the seven respective, concentrated zirconia suspensions to 5.7 μM, keeping the amount of dispersant equiproportional. Sodium chloride (99.99%, Alfa Aesar, USA) was added to each suspension at a concentration of 0.001 M; this addition acts as a buffer for pH adjustment and screening salt to fix electrostatic interactions. The pH was modified to 2, 4, 6, 8, 10, and 12 for solutions using HCl or NaOH (1 M, Alfa Aesar, USA) and a pH meter (HI5221, Hanna Instruments, Inc., Woonsocket, RI, USA). Before dispensing, solution bottles were mixed using a vortex mixer (Model No. 945404, Fisher Scientific) for approximately 60 s. Droplets of approximately 0.19 ± 0.02 mL were deposited onto borosilicate cover slips (22 ×30 mm, Corning Glass Works, Corning, NY, USA) using a disposable polyethylene transfer pipette (Fisherbrand, Fisher Scientific). Droplets were left to dry for approximately 8 h at 22 °C and 30% relative humidity.

2.2. Coffee-stain characterization and particulate characterization

The particle size distribution of the 24-hour milled zirconia was measured using laser diffraction (S3500, Microtrac Inc., Montgomeryville, PA, USA). Zeta potential was measured using electrophoresis (Zetasizer Nano ZS, Malvern Panalytical Ltd, Worcestershire, United Kingdom) for the 50 mg/g (3.125 mg/m^2) dispersant and distilled water solution. Macroscopic photos were taken with a consumer flatbed scanner (Photosmart 5525, HP). Two droplet deposits, one characteristic of a weakly flocculated suspension (approximately −30 mV zeta potential) and one with strongly dispersed particles (approximately −50 mV zeta potential), were selected for additional microstructural investigation using a scanning electron microscope (SEM; eLINE Plus, Raith GmbH, Germany). Images were captured using the secondary electron detector; operating parameters were a 1.5 kV accelerating voltage, 8 mm working distance, and a 30 μm aperture size.

2.3. Rheology

The rheology of concentrated zirconia pastes ($\varphi = 0.42$) containing 3.125 mg/m^2 of dispersant and 1% by volume (vol%) of cold water dispersible hydroxypropyl methylcellulose binder (HPMC; Methocel

J5M S, Dow Chemical Company, Midland, MI, USA), added to avoid sedimentation, were tested with a rotational rheometer (Kinexus Ultra+, Malvern Panalytical Ltd, Worcestershire, United Kingdom). A cone and plate (CP) geometry was utilized with a 40 mm cone diameter, 4° cone angle, and 150 μm gap at center. A solvent trap was used to minimize evaporation during tests. Oscillatory amplitude sweeps for the zirconia pastes of various volume fractions ($\varphi = 0.25–0.46$) were performed from 0.01% to 100% complex strain (corresponding to 0.1–1000 Pa complex stress for samples). Creep experiments were completed at stresses of 1–50 Pa to explore the possibility of delayed yielding in these systems. Before each creep test, samples were pre-sheared at 100 s^{-1} for 10 min followed by a recovery period of 10 min.

2.4. CODE printing – Paste preparation and printing parameters

Several paste compositions were prepared for CODE printing. The initial composition used for the gear in Fig. 1 consisted of 80.8 wt% TZ-3Y-E, 12.4 wt% distilled H_2O, 4.0 wt% Dolapix CE 64 dispersant, 2.4 wt % PEG 400 humectant, and 0.3 wt% Methocel J5M S binder. These correspond to respective volume percentages of approximately 42.2%, 39.3%, 10.6%, 6.8%, and 1.0%. For all pastes made for CODE printing, the zirconia slurries were prepared similar to Section 2.1 but with a higher solids loading (zirconia typically ~38–40 vol%), and were transferred to a 300 mL HDPE planetary mixing jar where HPMC and polyethylene glycol 400 (PEG 400; Carbowax, Dow Chemical Company, Midland, MI, USA; or similar) was added. Planetary mixing (ARE-310, THINKY Corporation, Japan) was completed at 2000 RPM until visibly homogeneous. To reach higher solids loadings, moisture was evaporated slowly with continuous planetary mixing to avoid film formation and particle aggregation. This paste was then degassed using a rough vacuum and transferred to a 50 mL Luer-Lock syringe tube using an electromagnetic jogger (J-1-B, Syntron Material Handling LLC, Tupelo, MS, USA) and vacuum syringe charger (ARC-40 H-300–55, THINKY Corporation, Japan). The tube was then loaded onto the CODE system, thus supplying paste to the CODE machine augers.

File preparation involved utilizing a commercial fused deposition modeling (FDM) stereolithography file (. STL) slicing software, Simplify3D (Version 4.0.0, Simplify3D, Cincinnati, OH), and a custom Python post-processing script. Printing was executed using the CODE system and a custom hardware abstraction layer (HAL), which expands upon the LinuxCNC (linuxcnc.org) real-time operating system. An electronic, auger-based dispenser (Preeflow ecoPEN 300, ViscoTec Inc., Kennesaw, GA, USA) was attached to the CODE 3-axis gantry which was controlled using a dosing system (eco-CONTROL EC200-K, ViscoTec Inc., Kennesaw, GA, USA). A standard gage precision nozzle (Subrex LLC, Carlsbad, CA, USA) with an inner diameter of 610 μm was used. Approximately 275 kPa (40 psi) of applied pressure was used to deliver paste to the electronic dispensers. Between 1.10 and 1.15 V were applied to the electronic dispenser corresponding to linear deposition rates of 0.22 mL/min. Travel speeds during extrusion were 1200 mm/min., and non-extruding gantry movement was set at 3600 mm/min. Deposited layers were nominally 300 μm thick. The gear, shown in Fig. 1(a), consisted of 115 layers and took approximately 4.5 h to complete. Similar parameters were utilized to produce other 3YSZ parts with sacrificial support materials [48]. Oil was applied around the part at the end of each new layer using a magnetic drive pump (2222-M04X06VC-O, Flight Works, Inc., Irvine, CA, USA). The oil level was held below the top-most layer to allow for adequate drying. Drying occurs either passively or actively using an infrared lamp fixed on a fourth, separate axis.

Printed parts were bulk dried in an environmental chamber (LH-1.5, Associated Environmental Systems, Ayer, MA, USA) at room temperature with approximately 70% relative humidity for 24 h. Binder removal and sintering took place in an electric furnace (DT-31, Deltech, Denver, CO, USA) and consisted of a 5 °C/min ramp to 450 °C, 2 h hold, 10 °C/min ramp to 1500 °C, and a final 1 h hold for densification before cooling at 10 °C/min.

3. Results and discussion

3.1. Ceramic on-demand extrusion

As introduced, CODE is a RC/DIW type process, but utilizes a rising oil bath, the level of which is kept below the top-most printed layers to minimize non-uniform drying. The use of this or a similar immiscible fluid bath can dramatically affect the final printed component strength. Despite limited material processing optimization, CODE printed, 3 mol % yttria stabilized zirconia (3YSZ) parts have exhibited densities > 99% and average flexural strengths of 715 MPa [43]. Additionally, because the typical mechanism of solidification or curing for CODE feedstocks after extrusion is drying, the use of an oil bath affects feedstock rheology; rheology is intertwined with overall 3D printability – a term which has many definitions [7,49,50]. To better understand the CODE process and how the oil bath modifies a typical DIW process, rheology, and ultimately feedstock printability – a schematic walkthrough of the paste rheology throughout CODE, or similar 3D printing processes, is shown in Fig. 2.

The elastic shear modulus (G′) and viscosity (η) are a function of primarily chemistry (μ), volume fraction (φ), shear rate ($\dot{\gamma}$), thixotropy ($\dot{\gamma}(t)$), and temperature (T). The paste viscosity changes greatly with respect to different parts of the printing process (i.e., time (t)). Before extrusion is initiated (0), the paste is primarily at rest, but likely flocculating over time to some degree. Once extrusion is initiated (1), the paste will flow through the confined flow path which increases shear and therefore decreases paste viscosity. Thixotropy can play a minor role here. Then, extrusion of the paste occurs at a shear rate specified by the nozzle diameter and volume extrusion rate (2). The paste will immediately start to recover (3) from shear and will also start to dry. Thixotropy, which is usually a minor effect in comparison to drying, will also reoccur. Over time (4), the printed layer will dry; this can be expediated by use of a heating lamp which can also act as a driving force for more uniform drying. After some amount of time, the layer is surrounded by oil (5). Ideally this layer is surrounded by oil when the rheology of the layer has become shear thickening for low shear rates (10^{-6} to 10^{-3} s^{-1}) due to partial drying. The layer should not be completely dried to retain plasticity and prevent oil ingress in the layer. The benefit of using an oil bath allows the layer to stay above the colloidal glass transition of the paste (φ_g) [51,52]. This allows the layers to slowly anneal or diffuse similar to traditional molecular glasses, provides for increased bonding between layers, and tends to reduce disorder and stresses (6). Ideally, the layers are kept at a moisture content that is above the point that shrinkage no longer occurs. For this study, the colloidal glass transition is roughly considered to be the critical moisture content (i.e., the inflection on a moisture content versus shrinkage plot). The part can then be removed from the build plate to avoid stresses related to adhesion and bulk drying (7). Two scenarios could have been occurring to cause particle migration, including (a) soft matter creep of the printed layers during the building of the part in regions (5) to (6) or (b) capillary migration of primary particles during post-processing (7). Because of this, both behaviors were investigated in the following sections to better understand the large defects occurring in this system.

3.2. Particle characterization and dilute coffee-ring effect study

The zirconia powders used to produce the pastes in this study have a bimodal particle size distribution with a d_{50} of ~0.3 μm and peaks at 170 and 490 nm (Fig. 3); a size ratio of approximately 2.88. Particle suspensions with wide or bimodal particle size distributions typically exhibit lower apparent viscosities than respective monodisperse suspensions [14,53,54]. Further, top-down milling processes have the tendency to form wider and bimodal distributions than bottom-up synthesis approaches [55].

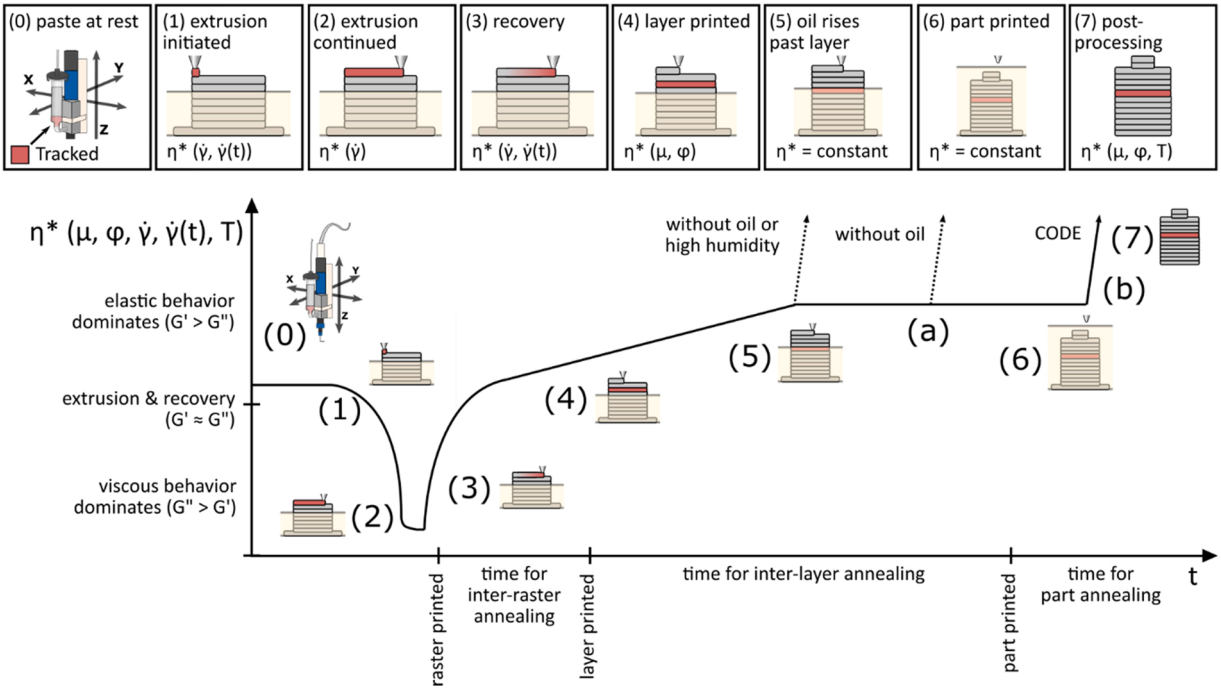

Fig. 2. Schematic of the relative viscosity versus time for the CODE process, distinguishing it from processes without the use of an immiscible fluid and pointing out regions (a) and (b) where particle migration could be occurring.

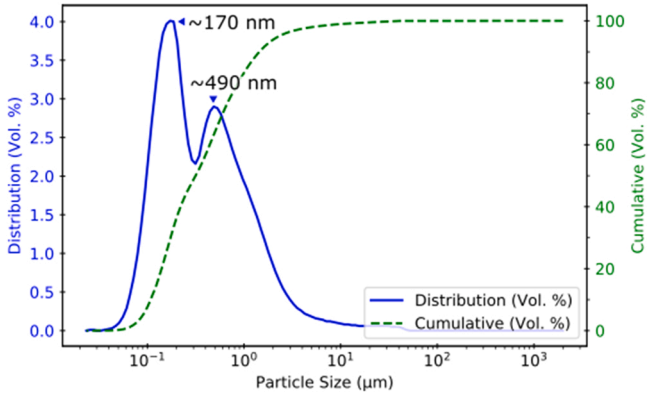

Fig. 3. Typical particle size distribution (by volume) for 24-hour, slow-milled TZ-3Y-E zirconia.

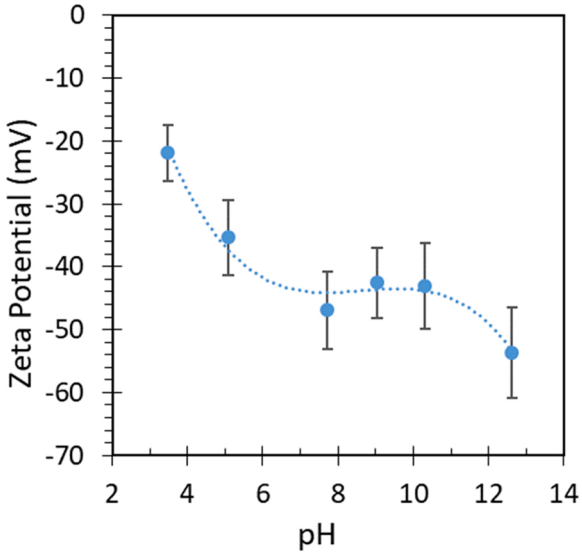

Fig. 4. Zeta potential measurements for TZ-3Y-E zirconia milled for 24 h with additions of 3.125 mg/m^2 (50 mg/g) of Dolapix CE 64 with respect to pH (dotted line as a guide).

As with most wet particulate processing and ceramic forming mechanisms, an organic dispersant was utilized to aid in particle dispersion by providing steric repulsion between particles [27]. The dispersant, Dolapix CE 64, is an alkali-free polycarbonic acid salt with a molecular weight of 300–400 g/mol. The zeta potential of a YSZ suspension with 3.125 mg/m^2 Dolapix CE 64 is shown in Fig. 4. The absolute value of the zeta potential increased with increasing pH with a plateau at slightly basic pHs. Rao et al. and Sarraf et al. investigated the effects of Dolapix CE 64 on sub-micron zirconia [56,57]. Their results compare favorably to the current study. Rao et. al. found that the zeta potential of zirconia shifted from 5.4 to 3.3 after the addition of 0.32 mg/m^2 (8 mg/g) of dispersant and considered this amount to be optimal. They also investigated the viscosity of 40 wt% zirconia suspensions and found that additional amounts of dispersant, 0.48 mg/m^2 (12 mg/g), continued to decrease the suspension viscosity without causing micelle formation or bridging flocculation. Due to the wide variability of zeta potential measurements, largely due to no established standard until recently [58], and because attractive forces are not considered, only loose trends were interpreted from zeta potential curves and the technical literature [59].

An overview of the characteristic coffee-ring (CR) deposits for solutions at different pH and dispersant concentrations is shown in Fig. 5. Various deposit morphologies are present. CR deposits from solutions with high pH and high dispersant concentration ((a), pH$>$ 7, $>$ 1.563 mg/m^2) exhibited a wide concentrated outer ring, an empty region, and inner striations. CR deposits from solutions with pH lower than neutral or lower dispersant concentration ((b), pH$\leq$ 7 or $<$ 0.625 mg/m^2) had a thin outer ring, a weakly populated intermediate region, and no inner striations. Highly acidic ((c), pH = 2) or basic ((d), pH= 12) solutions were dramatically affected by the chosen substrate borosilicate glass. Acidic solutions strongly wetted the substrate with a

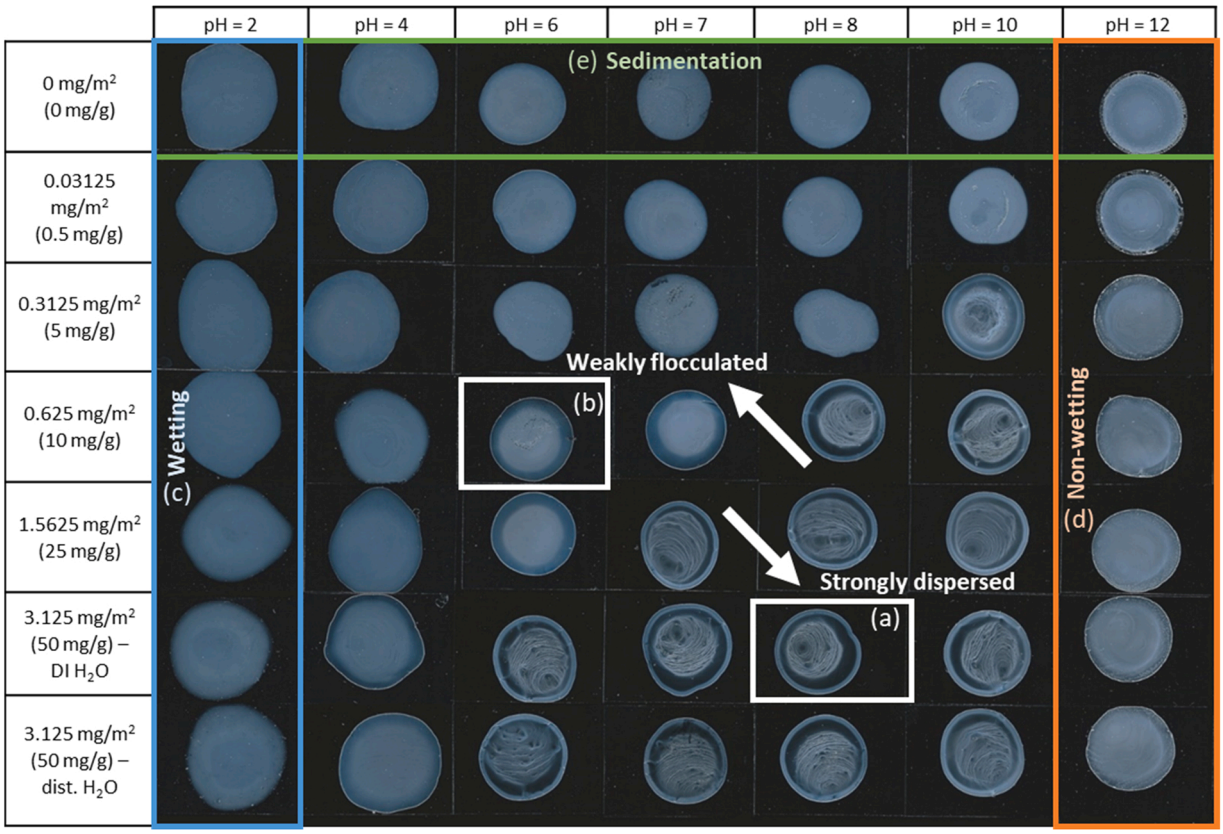

Fig. 5. Coffee-ring deposit morphology for various dispersant concentrations (rows) and pH (columns). Vertical deposits consisted of solutions with the same pH. Horizontal deposits consisted of solutions with the same concentration of Dolapix CE 64.

contact angle $< 45°$, thus pinning particles strongly at the outer edge. Basic solutions were less wetting (contact angle 45–90°) and minimized particles pinned at the outer edge due to inward flow. Solutions with low or no amounts of dispersant (e) formed particle deposits with roughly a half-ellipse shape as determined by contact profilometry, indicating particle sedimentation. Recirculating Marangoni flows compete with capillary flows and have been shown to redistribute particles inward to form coffee-ring eyes or small dots at the centers of deposits [60,61]. Some of this behavior is shown in the CR deposits in this study with high pH and high dispersant concentrations (pH>7, >1.563 mg/m^2, respectively).

As shown here in Fig. 5, and by Bhardwaj et al., the coffee-ring effect can be utilized to map Derjaguin-Landau-Verwey-Overbeek (DLVO) interactions with some considerations towards dispersants, pH, substrate chemistry, and fluid dynamics [62]. Similarly, the CR effect has shown promise for mapping behavior in a wide range of fields, including biomedical diagnostics and material development [63,64].

Some deposit morphologies observed in Fig. 5, such as the striations in deposits at high pH or dispersant concentrations (e.g., (a), pH> 7, > 1.563 mg/m^2, respectively) were unexpected. The microstructural features of a weakly flocculated sample ((b), pH = 6, 0.625 mg/m^2, zeta potential ~ -30 mV) and a strongly dispersed sample ((a), pH = 8, 3.125 mg/m^2, zeta potential ~ -50 mV) were subsequently examined via SEM (Fig. 6). The weakly flocculated sample (Fig. 6(a-c)) had particle arrangements which are characteristic of flocculated and dispersed microstructures in the center of the deposit (circled in Fig. 6(a)). These structures have been explored previously [65,66]. Outside the central region of the weakly flocculated sample (Fig. 6(b)), a thin, sparsely packed region exhibited flocculated structures. The deposit edge of the weakly flocculated sample (Fig. 6(c)) primarily contained strongly dispersed particles, evident by the high packing efficiency. However, the edge of the strongly dispersed sample (Fig. 6(d)) was more compact and defined, wicking most particles to the outer edge, and leaving a mostly empty region between the edge and central region (Fig. 6(e)). Long dendrites consisting of non-adsorbed dispersant were also observed in the middle region of the strongly dispersed sample representing diffusion limited aggregation in the sample (Fig. 6(e)). From the higher magnification it is evident that the striations in primarily the central regions of the strongly dispersed deposits are due to the bimodal particle size distribution (Fig. 6(f)). Clusters of ~490 nm particles were found in regions marked (1) while clusters of ~170 nm particles were found in regions marked (2). This is expected to have occurred due to the stick-slip phenomenon found previously, whereby a new contact line was formed due to the evaporation rate exceeding particle deposition [47,67].

3.3. Rheology

In order to probe the behavior of the concentrated zirconia pastes ($\varphi \gtrsim 0.25$), rotational shear rheology was performed. The rheology of concentrated ($\varphi = 0.25$–0.46) zirconia pastes with small amplitude oscillatory shear (SAOS) and creep tests were examined. At 42 vol% the pastes exhibited a G' of approximately 56,000 Pa and G" of 21,000 Pa in the linear viscoelastic region (LVER) (Fig. 7). In the intermediate non-linear regime (0.1–1% strain amplitude), a weak strain overshoot was exhibited [68]. This has been attributed to positive network parameters with a greater loss rate than creation rate (i.e., breakdown of connected structures such as flocs). The yield stress from small amplitude oscillatory shear is approximately 6–7 Pa (marked here by the beginning of the non-linear regime and the drop in G'). The flow stress (G'/G" = 1) is approximately 100 Pa. Logarithmic stress ramps exhibited yield stresses between 6 and 10 Pa. A Herschel-Bulkley model ($\tau = \tau_0 + K\dot{\gamma}^n$) can be fit with $\tau_0 = 7$ Pa, K = 61 Pa•s^n, and n = 0.26, where τ is the shear stress, τ_0 is the yield stress, K is consistency index, $\dot{\gamma}$ is shear rate, and n is flow

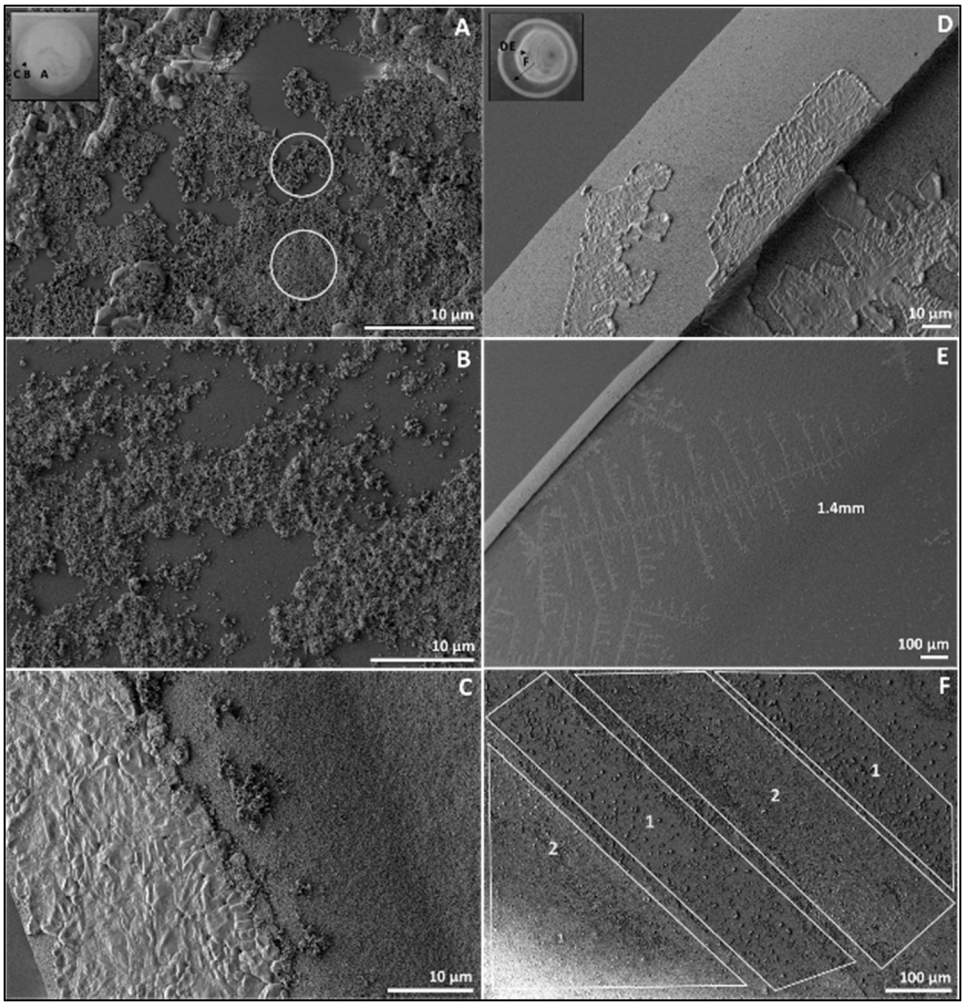

Fig. 6. Morphology of a weakly flocculated suspension deposit (zeta potential, −30 mV) (left) and of a strongly dispersed suspension deposit (right) (zeta potential, −50 mV). (A) Central region of the weakly flocculated deposit, (B) Sparsely packed middle region, (C) Deposit edge, (D) Deposit edge of the strongly dispersed sample, (E) Large dendrite of Dolapix CE 64 formed through diffusion-limited aggregation and central region void of particles (F) Stratification of the bimodal particle size distribution, (1) ~490 nm (2) ~170 nm.

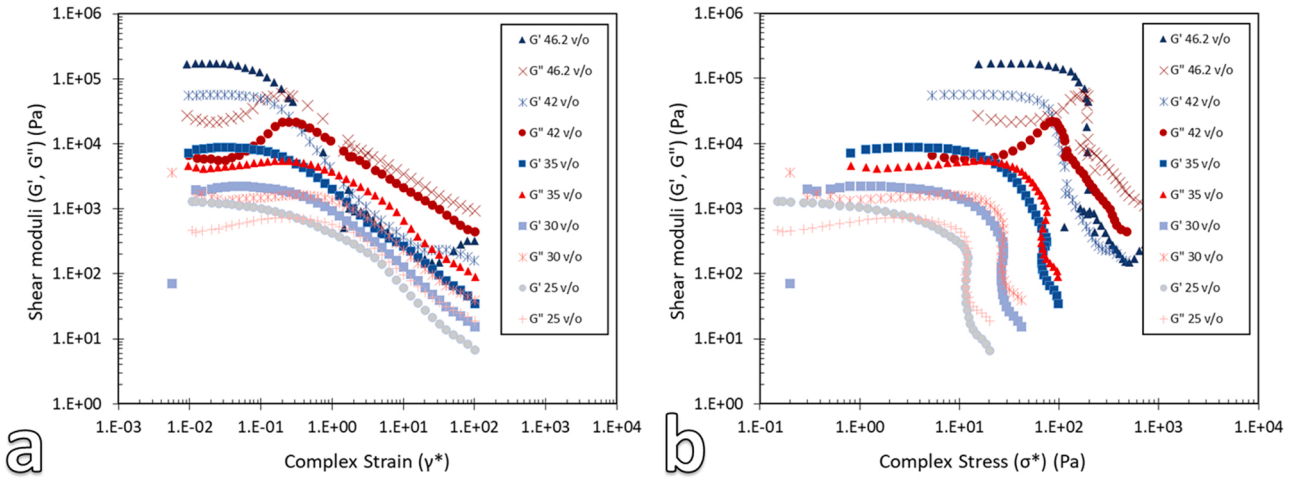

Fig. 7. Strain amplitude sweep for a concentrated (φ = 0.25–0.46) zirconia pastes. (a) Shear moduli versus complex strain, (b) Shear moduli versus complex stress demonstrating the increase in yield stress.

index. A flow index less than 1 indicates a shear thinning fluid, the consistency index can be used to compare the relative viscosity of fluids at low shear rates (1 s^{-1}), and the yield stress is the stress required to initiate flow, below which the fluid behaves elastically.

As an analogue to capillary and stress-driven migration, the creep of a concentrated zirconia paste was investigated for various applied stresses over time (Fig. 8). Creep of colloidal suspensions have three regions of response (schematic, Fig. 8a). Upon the application of an initial stress the material elastically deforms (1, i), followed by inertial ringing – characteristic of the elasticity of the sample and the rheometer coupling. In the second region (2), the material deviates depending on the applied stress (σ). For large stresses, the material instantly yields and

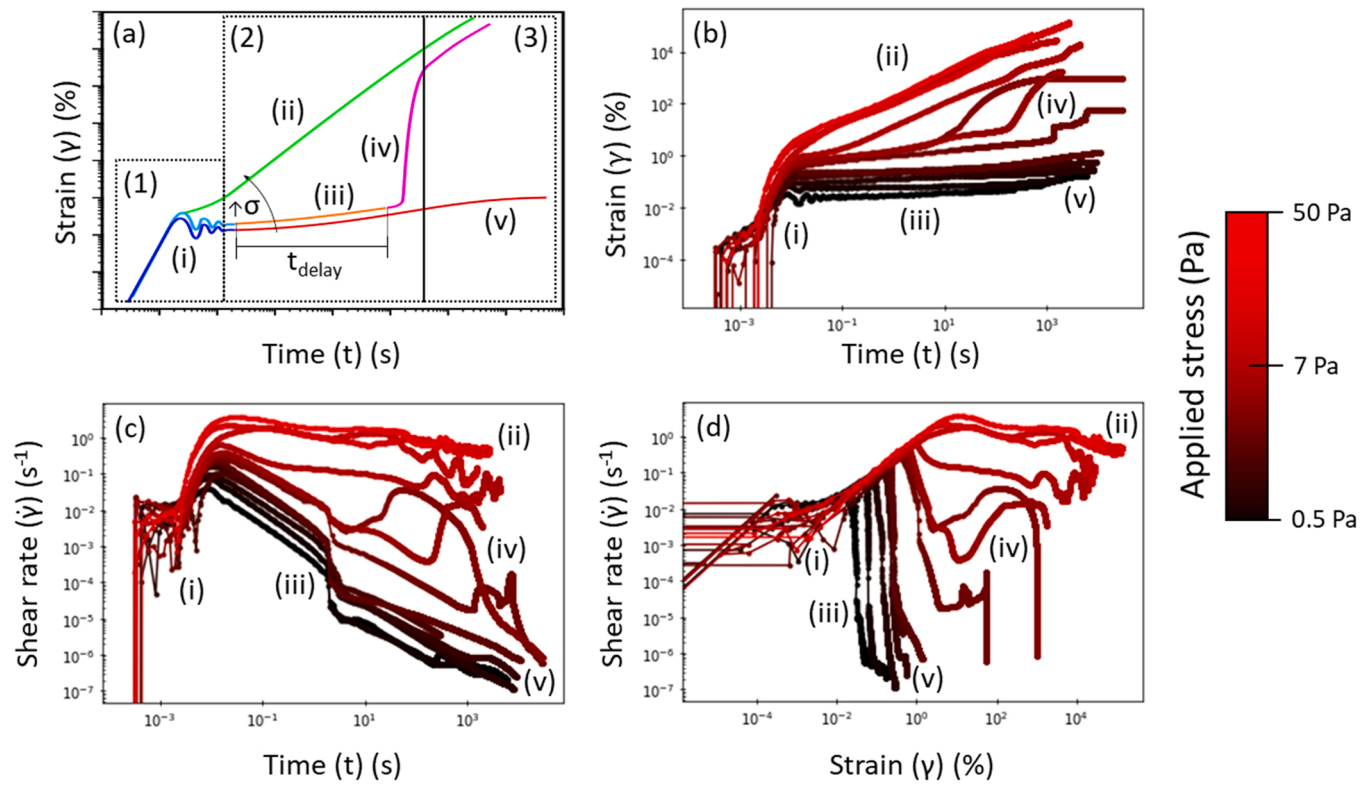

Fig. 8. (a) Schematic of characteristic creep responses for viscoelastic materials, (b) Creep response for a 42 vol% zirconia paste at 0.5–50 Pa applied stress, (c) Shear rate with respect to time, (d) Shear rate with respect to strain showing characteristic strain at the arrow.

linearly deforms over time (ii). For intermediate stresses, the material initially deforms at a uniform rate (iii), but catastrophically yields, or fails, after some delay time (t_{delay}) and strain build-up (iv). As stress is increased, the delay time decreases. For stresses lower than a critical stress ($\sigma_{critical}$), the gel slowly deforms following Andrade and alpha creep time dependence (v) for the allotted timeframe (~160 min). The third region (3) is dictated by the final response of the material – a viscous response where shear rate is constant (ii, iv) or linearly decays (v). From 2000–2020 this behavior has been explored, computationally and experimentally, and reviewed for a wide variety of colloidal systems [69–74].

As shown in Fig. 8b-d, for a strongly dispersed (pH = 10, dispersant concentration = 3.125 mg/m^2), concentrated ($\varphi = 0.42$) zirconia paste, stresses lower than 5 Pa exhibit no delayed yielding in the allotted time frame of 4 h. For stresses between 5 Pa and 10 Pa delayed yielding occurs at approximately 4–10% strain. For stresses greater than 10 Pa the paste immediately becomes more compliant over time. Under stresses and steady-state shear rates, directional structuring of the paste microstructure can occur. Eberle et al. utilized rheology coupled small-angle neutron scattering (rheo or flow-SANS) to observe this behavior in-situ [75]. Cipelletti et. al. utilized small angle light scattering to examine structural changes in the microstructure of creeping soft matter [76]. They found that there were considerably more dynamic bonds, and the occurrence of plastic rearrangements, that signaled the onset of delayed failure. They criticized molecular dynamic simulations due to the difficulty in simulating the slow, non-equilibrium microstructural dynamics of creep experiments and the accumulation of plastic events [77].

Again, to better understand the effect of paste rheology on defect formation in the larger cross-sections ceramic parts produced in this study, it is useful to examine where medium amplitude oscillatory shear (MAOS) and creep rheology is on Pipkin space [78]. As explored by Ewoldt and McKinley, these experiments primarily explore the intersection of viscometric, non-linear viscoelastic, linear viscoelastic, and Navier-Stokes flows and lie at the transition between solid and liquid-like behavior – the colloidal glass transition. As discussed, scientific challenges remain in the numerical and theoretical understanding of this transition, but recent experimental and computational approaches are promising [5,79,80]. Additionally, non-coupled rheological studies (including complementary compressive rheology, not explored here) can also still be utilized to approach these problems for the vast variety of practical systems [81,82].

3.4. Defect discussion

Since particle migration was mostly lateral and occurred after bulk drying, the primary mechanism causing the migration was expected to be due to capillary migration rather than creep. As discussed by Lewis et al., and similar to the coffee-ring effect or slip casting, it is suspected that CODE produced ceramic parts experienced pinning and drying of particles on the outside of the part first, thereby wicking particles away from the inner regions [27,66]. The similarity of this phenomenon to slip casting or the coffee-ring effect is promising for the CODE process and the use of an oil bath. It demonstrates that traditional behavior (and likely, properties) of slip cast objects can be found in CODE manufactured parts, eliminating the common perception that 3D printed parts cannot have comparable strengths to traditionally manufactured components (i.e., a perception of which SLA and related techniques have already been disproving for smaller, binder-loaded parts).

3.5. Calculations and paste adjustments

To understand the CODE process better, particularly for producing large, dense ceramic components, and to find methods for avoiding the particle migration that has been observed, the sintered zirconia gear was examined. The gear was 98.3% dense (5.95 g/cc of 6.05 g/cc (manufacturer)) from Archimedes density measurement (ASTM C373) [83]. Water was then added to the sintered cavity formed as an estimate of the volume of the defect. Approximately 0.44 mL in volume was needed to

fill the cavity. By compensating for the approximately 20% shrinkage during sintering, it was estimated that an additional ~3.8 vol% of solids would be required to avoid the cavity from forming or ~46 vol% ZrO_2 total for the paste formulation. Also of note is that this part was not removed from the build plate before bulk drying, therefore it experienced constrained shrinkage and stresses from slight adherence to the build substrate. The bottom of the sintered zirconia gear had a 0.70 ± 0.04° slope from gear teeth to its center.

Using previously establish heuristics by Lewis and Cima (Eq. 1), estimations of the effects of capillary migration for the CODE produced part were determined [15,27,66,84]. The length scale over which capillary migration should occur (l_{cap}), for Newtonian liquids derived from Darcy's law, is defined by H, the cast layer thickness, ΔP, the pressure difference between solvent saturated and dry regions estimated from Laplace capillary equation, φ, the solid volume fraction, V_E, the evaporation rate, η_0, the solution viscosity, A_s, the specific surface area, and ρ_s, the theoretical density of the solid particles.

$$l_{cap} = \left[\frac{2H(\Delta P)(1-\varphi)^3}{5V_E\eta_0(A_s\varphi\rho_s)^2}\right]^{\frac{1}{2}} \quad (1)$$

Using approximated values for our system (ΔP = 1.3 MPa, φ = 0.42, $V_E \approx 1.4\bullet10^{-7}$ $m^3/m^2\bullet s$, η_0 = 1 mPa•s, A_s = 16 m^2/g, ρ_s = 6.05 g/cc), and notably a large H (25.56 mm), a characteristic capillary length of 10.5 cm was calculated for the gear geometry. This is beyond the lateral dimensions of the printed object (~3.3 cm; 3.2 times smaller) which means that saturation uniformity conditions are achieved, avoiding dramatic stress build-up or cracking. However, excessively large values contribute to capillary-induced mass migration such as in coffee-rings, slip casting, and other similar processes. As another reference, typical values for l_{cap} for coffee-rings are approximately 100 times their lateral dimension which contributes to their prevalence. This criterion becomes especially important during the continual drive towards more precise deposition involving nanoparticle suspensions.

Using Eq. 1, modifications such as reducing the dispersant concentration from 50 mg/m^2 to 10 mg/m^2 (decrease of ΔP) (CRE results), increasing the solids loading from 42 to 46 vol% (φ) (part analysis & rheology), increasing the evaporation rate (V_E), or increasing the solution viscosity (i.e., curing or other timed processes) could assist in avoiding particle migration, and in avoiding modifications to the commercially important particulate.

3.6. Paste and process implications

To precisely create ceramic components, it is still necessary to establish rheological constraints or criteria for printable inks or pastes and ideally demonstrate predictive formulations for design [50,85]. It is also desirable to consolidate experimental validation to minimal different techniques; for most, this has been rotational shear rheology. Rogers et. al. utilized a series of physical processes (SPP) to establish these criteria for screen printing [86]. For reliable additive manufacturing it is also important to establish quality assurance measures and transition from part to process qualification to enable design freedom [5,87]. Further, there are also implications related to solvent design and for DIW processes which do not utilize a rising oil bath. Ideally diffusion is allowed between layers to provide for improved mechanical strengths, implying that the use of multiple liquid phases or solvents may aid in slowing the drying transition or more discretely transitioning between drying regimes. Additionally, the use of high humidity during printing or hydrogels keeps water retained in the paste for longer times. The effect diffusion has on mechanical strength has been explored for FDM printing [88]. For thermoplastic systems such as FDM or FDC this involves annealing above the glass transition temperature (Tg) by utilizing a heated build chamber, but also occurs slowly for the relatively high viscosities of polymers near Tg. For SLA, or similar stereolithography processes, a continuous interface is commonly used which allows for diffusion between layers despite partial curing [89,90].

Besides better inter-road and layer-layer bonding, lower solids loading feedstocks can also exhibit beneficial Orchard leveling [91,92] and greater fidelity if the lower pressures required enable the use of smaller nozzle diameters (lower ΔP_{drop} or clogging avoided). However, these are typically avoided due to increased shrinkage, poor structure (low G' or τ_{yield}) (both spanning and layer-layer building), poorer recovery (G' rebuild) causing excessive spreading or particle diffusion [93]. Excessively high shear rates or solids loadings can also cause surface fractures or shear banding during extrusion (i.e., limiting overall process speed) [94]. High solids loading pastes also have the problem of increased flocculation (lowered shelf life) due to a smaller interparticle spacing. Control of the interplay between diffusional and advective processes during forming and patterning is crucial – which is part of the reason 'programmable matter' or tunable rheology has been stressed in DIW [27,28,95,96].

Modifications of affecting the pressure differential (ΔP) to avoid migration during drying are also troublesome. Weakly and strongly flocculated microstructures can cause similar problems as increasing the solids loading. These adjustments also cause shear thixotropy and aging to be a more prominent phenomenon. Other authors suggest the use of an immiscible fluid during formulation to create capillary suspensions which effectively minimizes the pressure differential [97]. Although more practical to form, these microstructures limit the overall strength of the final printed part [98].

The paste printability, for the desired space-filling geometry (Fig. 1b), is subjectively, near optimal. Solids loading increases to 46 vol % were attempted, but this caused increased difficulty when preparing the feedstock (due to the proximity of shear thickening behavior at ~50 vol%) and during printing. Greater paste cohesion and normal forces caused an intolerance for even slight print height inconsistencies and caused paste stringing during rapid movements. Therefore, ideally process controls (i.e., increasing the evaporation rate (V_E) or solution viscosity with time (η_t)) are used to minimize defect formation during drying. Not explored in this study, this could involve the use of an IR or UV lamp to set the layer uniformly, partially after printing. Gel casting compositions also allow for targeted final solidification, but the avoidance of a large amount of polymer is necessary [99,100]. Timed coagulation printing (commonly direct coagulation casting (DCC)) is also a binder-less option, but solute segregation is exceptionally more difficult to solve than larger particles due to small Stokes radii (hydrodynamic radius of ~60 nm for 10^6 Da polymeric macromolecules) [27,101]. Therefore, compositional variations would need to be accounted for instead. Finally, similar process controls such as inducing Marangoni flows inside the part can likely help avoid the defect in analogies to CRE work [102].

4. Conclusion

In this study, drying defects that occur in Ceramic On-Demand Extrusion (CODE) components when printing densely filled, large continuous volume (≳ 1 cm^3) ceramic components consisting of ZrO_2 colloidal pastes (d_{50} ~0.3 μm) were investigated. The formation of this defect was directly influenced by the CODE process and demonstrates the possibility for mold-less slip casting. Printed parts exhibited lateral particle migration during post-processing.

Dilute suspensions of a commercial zirconia and dispersant were created to assess particle aggregation and microstructure. Particle aggregation effects were mapped with respect to pH and dispersant concentration. Highly packed structures were found in strongly dispersed (e.g., pH = 8, 3.125 mg/m^2, zeta potential ~ −50 mV) deposit microstructures and stratification of the bimodal particle size distribution was observed in these samples. Weakly flocculated deposits (e.g., pH = 6, 0.625 mg/m^2, zeta potential ~ −30 mV) exhibited looser packed edges and characteristic floc morphology.

Dispersed (pH = 10, 3.125 mg/m^2), concentrated (φ = 0.42)

zirconia pastes exhibited an elastic shear modulus (G') of 56,000 Pa and yield stresses between 6 and 10 Pa. These rheological properties allowed for builds of 34.5 mm in height over 115 layers without slumping due to partial drying, but these pastes demonstrated fluidization by delayed yielding behavior for stresses between 5 and 10 Pa when approximately 4–10% strain is accumulated.

Several methods were proposed to improve future feedstocks to prevent this defect based on the capillary length scale equation. Further, it was demonstrated that the CODE process effectively allows for layers to anneal while still allowing for precise layered printing, and implications of the colloidal glass transition were discussed. This work also brings about connections between inkjet and direct write printing and discusses desirable rheology towards the widespread goal of programmable patterning. Finally, this paper provides discourse to aid ceramic extrusion additive manufacturing design and processes. Further study is needed to accurately control and model the drying of suspensions during and after printing.

Declaration of Competing Interest

The authors declare that they have no known competing financial interests or personal relationships that could have appeared to influence the work reported in this paper.

Acknowledgements

This work was funded by Honeywell Federal Manufacturing and Technologies through contract number N000293380. Honeywell Federal Manufacturing and Technologies, LLC operates the Kansas City National Security Campus for the United States Department of Energy/National Nuclear Security Administration under contract number DE-NA0002839.

References

[1] N. Travitzky, A. Bonet, B. Dermeik, T. Fey, I. Filbert-Demut, L. Schlier, T. Schlordt, P. Greil, Additive manufacturing of ceramic-based materials, Adv. Eng. Mater. 16 (2014) 729–754, https://doi.org/10.1002/adem.201400097.
[2] A. Zocca, P. Colombo, C.M. Gomes, J. Günster, Additive manufacturing of ceramics: issues, potentialities, and opportunities, J. Am. Ceram. Soc. 98 (2015) 1983–2001, https://doi.org/10.1111/jace.13700.
[3] E. Peng, D. Zhang, J. Ding, Ceramic robocasting: recent achievements, potential, and future developments, Adv. Mater. 30 (2018), 1802404, https://doi.org/10.1002/adma.201802404.
[4] Z. Chen, Z. Li, J. Li, C. Liu, C. Lao, Y. Fu, C. Liu, Y. Li, P. Wang, Y. He, 3D printing of ceramics: a review, J. Eur. Ceram. Soc. 39 (2019) 661–687, https://doi.org/10.1016/J.JEURCERAMSOC.2018.11.013.
[5] A.J. Allen, I. Levin, S.E. Witt, Materials research & measurement needs for ceramics additive manufacturing, J. Am. Ceram. Soc. (2020), https://doi.org/10.1111/jace.17369.
[6] J.S. Pelz, N. Ku, M.A. Meyers, L.R. Vargas-Gonzalez, Additive manufacturing of structural ceramics: a historical perspective, J. Mater. Res. Technol. 15 (2021) 670–695, https://doi.org/10.1016/J.JMRT.2021.07.155.
[7] A. M'Barki, L. Bocquet, A. Stevenson, Linking rheology and printability for dense and strong ceramics by direct ink writing, Sci. Rep. 7 (2017) 6017, https://doi.org/10.1038/s41598-017-06115-0.
[8] M.N. Rahaman, Ceramic processing and sintering, M. Dekker, 2003. ⟨https://books.google.com/books/about/Ceramic_Processing_and_Sintering.html?id=5yERCU5miKkC⟩ (accessed August 26, 2018).
[9] G. Bandyopadhyay, K.W. French, Injection-molded ceramics: critical aspects of the binder removal process and component fabrication, J. Eur. Ceram. Soc. 11 (1993) 23–34, https://doi.org/10.1016/0955-2219(93)90055-V.
[10] E. Feilden, E.G.-T. Blanca, F. Giuliani, E. Saiz, L. Vandeperre, Robocasting of structural ceramic parts with hydrogel inks, J. Eur. Ceram. Soc. 36 (2016) 2525–2533, https://doi.org/10.1016/J.JEURCERAMSOC.2016.03.001.
[11] C.F. Revelo, H.A. Colorado, 3D printing of kaolinite clay ceramics using the direct ink writing (DIW) technique, Ceram. Int. 44 (2018) 5673–5682, https://doi.org/10.1016/j.ceramint.2017.12.219.
[12] C.J. Bae, J.W. Halloran, A segregation model study of suspension-based additive manufacturing, J. Eur. Ceram. Soc. 38 (2018) 5160–5166, https://doi.org/10.1016/j.jeurceramsoc.2018.07.008.
[13] C.-J. Bae, A. Ramachandran, J.W. Halloran, Quantifying particle segregation in sequential layers fabricated by additive manufacturing, J. Eur. Ceram. Soc. 38 (2018) 4082–4088, https://doi.org/10.1016/J.JEURCERAMSOC.2018.02.008.
[14] C.-J. Bae, J.W. Halloran, Concentrated suspension-based additive manufacturing – viscosity, packing density, and segregation, J. Eur. Ceram. Soc. 39 (2019) 4299–4306, https://doi.org/10.1016/j.jeurceramsoc.2019.05.034.
[15] M.J. Cima, J.A. Lewis, A.D. Devoe, Binder distribution in ceramic greenware during thermolysis, J. Am. Ceram. Soc. 72 (1989) 1192–1199, https://doi.org/10.1111/j.1151-2916.1989.tb09707.x.
[16] A. Poitou, G. Racineux, A squeezing experiment showing binder migration in concentrated suspensions, J. Rheol. 45 (2001) 609–625, https://doi.org/10.1122/1.1366717.
[17] W.J. Costakis, L.M. Rueschhoff, A.I. Diaz-Cano, J.P. Youngblood, R.W. Trice, Additive manufacturing of boron carbide via continuous filament direct ink writing of aqueous ceramic suspensions, J. Eur. Ceram. Soc. 36 (2016) 3249–3256, https://doi.org/10.1016/J.JEURCERAMSOC.2016.06.002.
[18] S. Wu, S. Rangarajan, C. Dai, R. McCuiston, N.A. Langrana, A. Safari, S. C. Danforth, R.B. Clancy, P.J. Whalen, Warm isostatic pressing (WIP'ing) of GS44 Si3N4 FDC parts for defect removal, Mater. Des. 24 (2003) 681–686, https://doi.org/10.1016/S0261-3069(01)00038-3.
[19] L. Rueschhoff, W. Costakis, M. Michie, J. Youngblood, R. Trice, Additive manufacturing of dense ceramic parts via direct ink writing of aqueous alumina suspensions, Int. J. Appl. Ceram. Technol. 13 (2016) 821–830, https://doi.org/10.1111/ijac.12557.
[20] T.L. Jones, L.R. Vargas-Gonzalez, B. Scott, B. Goodman, B. Becker, Ballistic evaluation and damage characterization of 3–D printed, alumina-based ceramics for light armor applications, Int. J. Appl. Ceram. Technol. 17 (2020) 424–437, https://doi.org/10.1111/ijac.13428.
[21] J. Cesarano, B.H. King, H.B. Denham, J. Cesarano III, H.B. Denham, Recent Developments in Robocasting of Ceramics and Multimaterial Deposition, Proceedings of Solid Freeform Fabrication Symposium. (1998) 697–703. ⟨http://www.osti.gov/servlets/purl/290950-XqAzAx/webviewable/%5Cn%3CGotoISI%3E://WOS:000082420400080⟩.
[22] J. Zheng, J.S. Reed, Particle and granule parameters affecting compaction efficiency in dry pressing, J. Am. Ceram. Soc. 71 (1988) C456–C458, https://doi.org/10.1111/j.1151-2916.1988.tb07546.x.
[23] H. Zipse, Finite-element simulation of the die pressing and sintering of a ceramic component, J. Eur. Ceram. Soc. 17 (1997) 1707–1713, https://doi.org/10.1016/s0955-2219(97)00037-x.
[24] K.G. Ewsuk, J.G. Arguello, D.N. Bencoe, D.T. Ellerby, S.J. Glass, D.H. Zeuch, J. Anderson, Characterizing Granulated Ceramic Powders for Dry Pressing and Sintering, John Wiley & Sons, Ltd,, 2012, pp. 77–88, https://doi.org/10.1002/9781118371480.ch11 (in:).
[25] F.F. Lange, Powder processing science and technology for increased reliability, J. Am. Ceram. Soc. 72 (1989) 3–15, https://doi.org/10.1111/j.1151-2916.1989.tb05945.x.
[26] W.M. Sigmund, N.S. Bell, L. Bergström, Novel powder-processing methods for advanced ceramics, J. Am. Ceram. Soc. 83 (2000) 1557–1574, https://doi.org/10.1111/j.1151-2916.2000.tb01432.x.
[27] J.A. Lewis, Colloidal processing of ceramics, J. Am. Ceram. Soc. 83 (2004) 2341–2359, https://doi.org/10.1111/j.1151-2916.2000.tb01560.x.
[28] G.V. Franks, C. Tallon, A.R. Studart, M.L. Sesso, S. Leo, Colloidal processing: enabling complex shaped ceramics with unique multiscale structures, J. Am. Ceram. Soc. 100 (2017) 458–490, https://doi.org/10.1111/jace.14705.
[29] R. Moreno, Better ceramics through colloid chemistry, J. Eur. Ceram. Soc. 40 (2019) 559–587, https://doi.org/10.1016/J.JEURCERAMSOC.2019.10.014.
[30] J.W. Halloran, Ceramic stereolithography: additive manufacturing for ceramics by photopolymerization, Annu. Rev. Mater. Res. 46 (2016) 19–40, https://doi.org/10.1146/annurev-matsci-070115-031841.
[31] J. Gonzalez-Gutierrez, S. Cano, S. Schuschnigg, C. Kukla, J. Sapkota, C. Holzer, Additive manufacturing of metallic and ceramic components by the material extrusion of highly-filled polymers: a review and future perspectives, Materials 11 (2018) 840, https://doi.org/10.3390/ma11050840.
[32] X. Lv, F. Ye, L. Cheng, S. Fan, Y. Liu, Binder jetting of ceramics: powders, binders, printing parameters, equipment, and post-treatment, Ceram. Int. 45 (2019) 12609–12624, https://doi.org/10.1016/j.ceramint.2019.04.012.
[33] A. Mostafaei, A.M. Elliott, J.E. Barnes, F. Li, W. Tan, C.L. Cramer, P. Nandwana, M. Chmielus, Binder jet 3D printing – process parameters, materials, properties, and challenges, Prog. Mater. Sci. (2020), 100707, https://doi.org/10.1016/j.pmatsci.2020.100707.
[34] J.W. Choi, H.C. Kim, R. Wicker, Multi-material stereolithography, J. Mater. Process. Technol. 211 (2011) 318–328, https://doi.org/10.1016/j.jmatprotec.2010.10.003.
[35] A. Bandyopadhyay, B. Heer, Additive manufacturing of multi-material structures, Mater. Sci. Eng.: R: Rep. 129 (2018) 1–16, https://doi.org/10.1016/J.MSER.2018.04.001.
[36] M. Wehner, R.L. Truby, D.J. Fitzgerald, B. Mosadegh, G.M. Whitesides, J. A. Lewis, R.J. Wood, An integrated design and fabrication strategy for entirely soft, autonomous robots, Nature 536 (2016) 451–455, https://doi.org/10.1038/nature19100.
[37] F. Alkadi, K.C. Lee, A.H. Bashiri, J.W. Choi, Conformal additive manufacturing using a direct-print process, Addit. Manuf. 32 (2020), 100975, https://doi.org/10.1016/j.addma.2019.100975.
[38] J.J. Adams, E.B. Duoss, T.F. Malkowski, M.J. Motala, B.Y. Ahn, R.G. Nuzzo, J. T. Bernhard, J.A. Lewis, Conformal printing of electrically small antennas on three-dimensional surfaces, Adv. Mater. 23 (2011) 1335–1340, https://doi.org/10.1002/adma.201003734.
[39] J.F. Destino, N.A. Dudukovic, M.A. Johnson, D.T. Nguyen, T.D. Yee, G.C. Egan, A. M. Sawvel, W.A. Steele, T.F. Baumann, E.B. Duoss, T. Suratwala, R. Dylla-Spears,

3D printed optical quality silica and silica-titania glasses from sol-gel feedstocks, Adv. Mater. Technol. 3 (2018), 1700323, https://doi.org/10.1002/admt.201700323.
[40] W. Li, A. Armani, A. Martin, B. Kroehler, A. Henderson, T. Huang, J. Watts, G. Hilmas, M. Leu, Extrusion-based additive manufacturing of functionally graded ceramics, J. Eur. Ceram. Soc. (2020), https://doi.org/10.1016/j.jeurceramsoc.2020.10.029.
[41] J.S. Pelz, N. Ku, W.T. Shoulders, M.A. Meyers, L.R. Vargas-Gonzalez, Multi-material additive manufacturing of functionally graded carbide ceramics via active, in-line mixing, Addit. Manuf. 37 (2021), 101647, https://doi.org/10.1016/j.addma.2020.101647.
[42] J.E. Smay, J. Cesarano, J.A. Lewis, Colloidal inks for directed assembly of 3-D periodic structures, Langmuir 18 (2002) 5429–5437, https://doi.org/10.1021/la0257135.
[43] W. Li, A. Ghazanfari, D. McMillen, M.C. Leu, G.E. Hilmas, J. Watts, Characterization of zirconia specimens fabricated by ceramic on-demand extrusion, Ceram. Int. 44 (2018) 12245–12252, https://doi.org/10.1016/j.ceramint.2018.04.008.
[44] M.C. Leu, A. Ghazanfari, W. Li, G.E. Hilmas, R.G. Landers, Method and apparatus for fabricating ceramic and metal components via additive manufacturing with uniform layered radiation drying, US10259158B2, 2016.
[45] A. Ghazanfari, W. Li, M.C. Leu, G.E. Hilmas, A novel freeform extrusion fabrication process for producing solid ceramic components with uniform layered radiation drying, Addit. Manuf. 15 (2017) 102–112, https://doi.org/10.1016/J.ADDMA.2017.04.001.
[46] R.D. Deegan, O. Bakajin, T.F. Dupont, G. Huber, S.R. Nagel, T.A. Witten, Capillary flow as the cause of ring stains from dried liquid drops, Nature 389 (1997) 827–829, https://doi.org/10.1038/39827.
[47] D. Mampallil, H.B. Eral, A review on suppression and utilization of the coffee-ring effect, Adv. Colloid Interface Sci. 252 (2018) 38–54, https://doi.org/10.1016/J.CIS.2017.12.008.
[48] W. Li, A. Armani, D. McMillen, M. Leu, G. Hilmas, J. Watts, Additive manufacturing of zirconia parts with organic sacrificial supports, Int. J. Appl. Ceram. Technol. 17 (2020) 1544–1553, https://doi.org/10.1111/ijac.13520.
[49] C. Duty, C. Ajinjeru, V. Kishore, B. Compton, N. Hmeidat, X. Chen, P. Liu, A. A. Hassen, J. Lindahl, V. Kunc, What makes a material printable? A viscoelastic model for extrusion-based 3D printing of polymers, J. Manuf. Process. 35 (2018) 526–537, https://doi.org/10.1016/J.JMAPRO.2018.08.008.
[50] N.A. Dudukovic, L.L. Wong, D.T. Nguyen, J.F. Destino, T.D. Yee, F.J. Ryerson, T. Suratwala, E.B. Duoss, R. Dylla-Spears, Predicting nanoparticle suspension viscoelasticity for multimaterial 3D printing of silica–titania glass, ACS Appl. Nano Mater. 1 (2018) 4038–4044, https://doi.org/10.1021/acsanm.8b00821.
[51] E.R. Weeks, Introduction to the colloidal glass transition, ACS Macro Lett. (2017), https://doi.org/10.1021/acsmacrolett.6b00826.
[52] G.L. Hunter, E.R. Weeks, The physics of the colloidal glass transition, Rep. Prog. Phys. 75 (2012), 066501, https://doi.org/10.1088/0034-4885/75/6/066501.
[53] J.E. Funk, D.R. Dinger, Predictive Process Control of Crowded Particulate Suspensions, Springer, US, Boston, MA, 1994, https://doi.org/10.1007/978-1-4615-3118-0.
[54] C.J. Martinez, J.A. Lewis, Rheological, structural, and stress evolution of aqueous Al2O3: latex tape-cast layers, J. Am. Ceram. Soc. 85 (2002) 2409–2416, https://doi.org/10.1111/j.1151-2916.2002.tb00473.x.
[55] G.L. Güngör, A. Kara, M. Blosi, D. Gardini, G. Guarini, C. Zanelli, M. Dondi, Micronizing ceramic pigments for inkjet printing: Part I. Grindability and particle size distribution, Ceram. Int. 41 (2015) 6498–6506, https://doi.org/10.1016/J.CERAMINT.2015.01.093.
[56] S.P. Rao, S.S. Tripathy, A.M. Raichur, Dispersion studies of sub-micron zirconia using Dolapix CE 64, Colloids Surf. A: Physicochem. Eng. Asp. 302 (2007) 553–558, https://doi.org/10.1016/J.COLSURFA.2007.03.034.
[57] H. Sarraf, Z. Qian, L. Škarpová, B. Wang, R. Herbig, M. Maryška, L. Bartovska, J. Havrda, B. Anvari, Direct probing of dispersion quality of ZrO2 nanoparticles coated by polyelectrolyte at different concentrated suspensions, Nanoscale Res. Lett. (2015), https://doi.org/10.1186/s11671-015-1157-z.
[58] NIST Collaboration Yields First Certified Reference Materials for Zeta Potential | NIST, (n.d.). ⟨https://www.nist.gov/news-events/news/2021/01/nist-collaboration-yields-first-certified-reference-materials-zeta⟩.
[59] S. Bhattacharjee, DLS and zeta potential – what they are and what they are not? J. Control. Release 235 (2016) 337–351, https://doi.org/10.1016/J.JCONREL.2016.06.017.
[60] E.L. Talbot, H.N. Yow, L. Yang, A. Berson, S.R. Biggs, C.D. Bain, Printing small dots from large drops, ACS Appl. Mater. Interfaces 7 (2015) 3782–3790, https://doi.org/10.1021/am5087177.
[61] Y. Li, C. Lv, Z. Li, D. Quéré, Q. Zheng, From coffee rings to coffee eyes, Soft Matter 11 (2015) 4669–4673, https://doi.org/10.1039/C5SM00654F.
[62] R. Bhardwaj, X. Fang, P. Somasundaran, D. Attinger, Self-assembly of colloidal particles from evaporating droplets: role of DLVO interactions and proposition of a phase diagram, Langmuir 26 (2010) 7833–7842, https://doi.org/10.1021/la9047227.
[63] R. Chen, L. Zhang, D. Zang, W. Shen, Blood drop patterns: formation and applications, Adv. Colloid Interface Sci. 231 (2016) 1–14, https://doi.org/10.1016/J.CIS.2016.01.008.
[64] L.F. Chen, J.R.G. Evans, Spontaneous manufacturing: alumina 128-well plates made by droplet drying, Adv. Appl. Ceram. 109 (2010) 51–55, https://doi.org/10.1179/174367609X456020.
[65] J.S. Abel, G.C. Stangle, C.H. Schilling, I.A. Aksay, Sedimentation in flocculating colloidal suspensions, J. Mater. Res. 9 (1994) 451–461, https://doi.org/10.1557/JMR.1994.0451.
[66] J.J. Guo, J.A. Lewis, Aggregation effects on the compressive flow properties and drying behavior of colloidal silica suspensions, J. Am. Ceram. Soc. 82 (1999) 2345–2358, https://doi.org/10.1111/j.1151-2916.1999.tb02090.x.
[67] C. Seo, D. Jang, J. Chae, S. Shin, Altering the coffee-ring effect by adding a surfactant-like viscous polymer solution, Sci. Rep. 7 (2017) 500, https://doi.org/10.1038/s41598-017-00497-x.
[68] K. Hyun, M. Wilhelm, C.O. Klein, K.S. Cho, J.G. Nam, K.H. Ahn, S.J. Lee, R. H. Ewoldt, G.H. McKinley, A review of nonlinear oscillatory shear tests: Analysis and application of large amplitude oscillatory shear (LAOS, Prog. Polym. Sci. (Oxf.) 36 (2011) 1697–1753, https://doi.org/10.1016/j.progpolymsci.2011.02.002.
[69] M. Siebenbürger, M. Ballauff, Th Voigtmann, Creep in colloidal glasses, Phys. Rev. Lett. 108 (2012), 255701, https://doi.org/10.1103/PhysRevLett.108.255701.
[70] P. Lidon, L. Villa, S. Manneville, Power-law creep and residual stresses in a carbopol gel, Rheol. Acta 56 (2017) 307–323, https://doi.org/10.1007/s00397-016-0961-4.
[71] M. Vandamme, F.-J. Ulm, Nanogranular origin of concrete creep, Proc. Natl. Acad. Sci. USA 106 (2009) 10552–10557, https://doi.org/10.1073/pnas.0901033106.
[72] L.J. Teece, J.M. Hart, K.Y.N. Hsu, S. Gilligan, M.A. Faers, P. Bartlett, Gels under stress: the origins of delayed collapse, Colloids Surf. A: Physicochem. Eng. Asp. (2014), https://doi.org/10.1016/j.colsurfa.2014.03.018.
[73] J. Sprakel, S.B. Lindström, T.E. Kodger, D.A. Weitz, Stress enhancement in the delayed yielding of colloidal gels, Phys. Rev. Lett. 106 (2011), 248303, https://doi.org/10.1103/PhysRevLett.106.248303.
[74] T. Gibaud, T. Divoux, S. Manneville, Nonlinear mechanics of colloidal gels: creep, fatigue and shear-induced yielding, Encycl. Complex. Syst. Sci. (2020) 1–24, https://doi.org/10.1007/978-3-642-27737-5_743-1.
[75] A.P.R. Eberle, N. Martys, L. Porcar, S.R. Kline, W.L. George, J.M. Kim, P.D. Butler, N.J. Wagner, Shear viscosity and structural scalings in model adhesive hard-sphere gels, Phys. Rev. E 89 (2014), 050302, https://doi.org/10.1103/PhysRevE.89.050302.
[76] S. Aime, L. Ramos, L. Cipelletti, Microscopic dynamics and failure precursors of a gel under mechanical load, Proc. Natl. Acad. Sci. USA 115 (2018) 3587–3592, https://doi.org/10.1073/pnas.1717403115.
[77] L. Cipelletti, K. Martens, L. Ramos, Microscopic precursors of failure in soft matter, Soft Matter 16 (2019) 82–93, https://doi.org/10.1039/c9sm01730e.
[78] R.H. Ewoldt, G.H. McKinley, Mapping thixo-elasto-visco-plastic behavior, Rheol. Acta 56 (2017) 195–210, https://doi.org/10.1007/s00397-017-1001-8.
[79] D.R. Cassar, ViscNet: neural network for predicting the fragility index and the temperature-dependency of viscosity, Acta Mater. 206 (2021), 116602, https://doi.org/10.1016/j.actamat.2020.116602.
[80] Ravinder, V. Venugopal, S. Bishnoi, S. Singh, M. Zaki, H.S. Grover, M. Bauchy, M. Agarwal, N.M.A. Krishnan, Artificial intelligence and machine learning in glass science and technology: 21 challenges for the 21st century, Int. J. Appl. Glass Sci. (2021), https://doi.org/10.1111/ijag.15881 ijag.15881.
[81] G.M. Channell, C.F. Zukoski, Shear and compressive rheology of aggregated alumina suspensions, AIChE J. 43 (1997) 1700–1708, https://doi.org/10.1002/aic.690430707.
[82] V. Gopalakrishnan, C.F. Zukoski, Delayed flow in thermo-reversible colloidal gels, J. Rheol. 51 (2007) 623–644, https://doi.org/10.1122/1.2736413.
[83] ASTM International, ASTM C373-18: Standard Test Methods for Determination of Water Absorption and Associated Properties by Vacuum Method for Pressed Ceramic Tiles and Glass Tiles and Boil Method for Extruded Ceramic Tiles and Non-tile Fired Ceramic Whiteware Products, ASTM International, 2018, p. 7.
[84] J.J. Guo, Aggregation effects on the rheological sedimentation and drying behavior of colloidal silica suspensions, University of Illinois at Urbana-Champaign, 1998.
[85] R.J. Flatt, P. Bowen, Yodel: a yield stress model for suspensions, J. Am. Ceram. Soc. 89 (2006) 1244–1256, https://doi.org/10.1111/j.1551-2916.2005.00888.x.
[86] G.J. Donley, W.W. Hyde, S.A. Rogers, F. Nettesheim, Yielding and recovery of conductive pastes for screen printing, Rheol. Acta 58 (2019) 361–382, https://doi.org/10.1007/s00397-019-01148-w.
[87] M. Seifi, A. Salem, J. Beuth, O. Harrysson, J.J. Lewandowski, Overview of materials qualification needs for metal additive manufacturing, JOM 68 (2016) 747–764, https://doi.org/10.1007/s11837-015-1810-0.
[88] T.J. Coogan, D.O. Kazmer, Bond and part strength in fused deposition modeling, Rapid Prototyp. J. 23 (2017) 414–422, https://doi.org/10.1108/RPJ-03-2016-0050.
[89] J.R. Tumbleston, D. Shirvanyants, N. Ermoshkin, R. Janusziewicz, A.R. Johnson, D. Kelly, K. Chen, R. Pinschmidt, J.P. Rolland, A. Ermoshkin, E.T. Samulski, J. M. DeSimone, Continuous liquid interface production of 3D objects, Science 347 (2015) (1979) 1349–1352, https://doi.org/10.1126/science.aaa2397.
[90] D.A. Walker, J.L. Hedrick, C.A. Mirkin, Rapid, large-volume, thermally controlled 3D printing using a mobile liquid interface, Science 366 (2019) (1979) 360–364, https://doi.org/10.1126/science.aax1562.
[91] R.R. Iyer, D.W. Bousfield, The leveling of coating defects with shear thinning rheology, Chem. Eng. Sci. 51 (1996) 4611–4617, https://doi.org/10.1016/0009-2509(96)00318-1.
[92] F. Seeler, C. Hager, O. Tiedje, M. Schneider, Simulations and experimental investigation of paint film leveling, J. Coat. Technol. Res. 14 (2017) 767–781, https://doi.org/10.1007/s11998-017-9934-5.

[93] S.S.L. Chan, M.L. Sesso, G.V. Franks, Direct ink writing of hierarchical porous alumina-stabilized emulsions: rheology and printability, J. Am. Ceram. Soc. 103 (2020) 5554–5566, https://doi.org/10.1111/jace.17305.
[94] J. Benbow, J. Bridgwater, Paste Flow and Extrusion, Clarendon Press, 1993.
[95] K.T. Faber, T. Asefa, M. Backhaus-Ricoult, R. Brow, J.Y. Chan, S. Dillon, W. G. Fahrenholtz, M.W. Finnis, J.E. Garay, R.E. García, Y. Gogotsi, S.M. Haile, J. Halloran, J. Hu, L. Huang, S.D. Jacobsen, E. Lara-Curzio, J. LeBeau, W.E. Lee, C.G. Levi, I. Levin, J.A. Lewis, D.M. Lipkin, K. Lu, J. Luo, J.-P. Maria, L.W. Martin, S. Martin, G. Messing, A. Navrotsky, N.P. Padture, C. Randall, G.S. Rohrer, A. Rosenflanz, T.A. Schaedler, D.G. Schlom, A. Sehirlioglu, A.J. Stevenson, T. Tani, V. Tikare, S. Trolier-McKinstry, H. Wang, B. Yildiz, The role of ceramic and glass science research in meeting societal challenges: Report from an NSF-sponsored workshop, J. Am. Ceram. Soc. 100 (2017) 1777–1803, https://doi.org/10.1111/jace.14881.
[96] C. Zhu, A.J. Pascall, N. Dudukovic, M.A. Worsley, J.D. Kuntz, E.B. Duoss, C. M. Spadaccini, Colloidal Materials for 3D Printing, Annu. Rev. Chem. Biomol. Eng. 10 (2019), https://doi.org/10.1146/annurev-chembioeng-060718-030133.
[97] S.B. Fischer, E. Koos, Using an added liquid to suppress drying defects in hard particle coatings, J. Colloid Interface Sci. 582 (2021) 1231–1242, https://doi.org/10.1016/j.jcis.2020.08.055.
[98] K. Kendall, N.M.N. Alford, W.J. Clegg, J.D. Birchall, Flocculation clustering and weakness of ceramics, Nature 339 (1989) 130–132, https://doi.org/10.1038/339130a0.
[99] M. Janney, Gelcasting - a new way to form large near-net-shape ceramic parts, Mater. Technol. 9 (1994) 97–99, https://doi.org/10.1080/10667857.1994.11785035.
[100] R. Gilissen, J.P. Erauw, A. Smolders, E. Vanswijgenhoven, J. Luyten, Gelcasting, a near net shape technique, Mater. Des. 21 (2000) 251–257, https://doi.org/10.1016/s0261-3069(99)00075-8.
[101] D.H. Napper, Polymeric Stabilization of Colloidal Dispersions, Academic Press, 1983.
[102] H. Hu, R.G. Larson, Marangoni effect reverses coffee-ring depositions, J. Phys. Chem. B. 110 (2006) 7090–7094, https://doi.org/10.1021/jp0609232.